

A Potential Energy Landscape Study of the Amorphous-Amorphous Transformation in H₂O

Nicolas Giovambattista¹, H. Eugene Stanley¹ and Francesco Sciortino²

¹*Center for Polymer Studies and Department of Physics,
Boston University, Boston, MA 02215 USA*

²*Dipartimento di Fisica and INFN Udr and Center for Statistical Mechanics and Complexity,
Universita' di Roma "La Sapienza"*

Piazzale Aldo Moro 2, I-00185, Roma, Italy

(Dated: Received 21 Feb 2003, Revised 5 June 2003. — LB9394 —)

We study the potential energy landscape explored during a compression-decompression cycle for the SPC/E (extended simple point charge) model of water. During the cycle, the system changes from low density amorphous ice (LDA) to high density amorphous ice (HDA). After the cycle, the system does not return to the same region of the landscape, supporting the interesting possibility that more than one significantly different configuration corresponds to LDA. We find that the regions of the landscape explored during this transition have properties remarkably different from those explored in thermal equilibrium in the liquid phase.

The physics of water in its supercooled and glassy phases is the object of several recent experimental [1, 2, 3, 4, 5, 6] and theoretical [7, 8, 9, 10] investigations. One of the most fascinating aspects is the possibility of a liquid-liquid phase transition [8] and the relation between the two liquid phases and the glassy phases of water [9]. These glassy phases are produced via routes as different as crystal compression, hyper-quenching, and vapor deposition, and are characterized by different densities and by different local structures [4, 5, 11]. The intrinsic out-of-equilibrium nature of these phases leads to some ambiguities in the identification of the materials produced via different routes, and recent debate concerns the classification of the different amorphous structures found [3, 4, 5, 6]. High density amorphous ice (HDA) resulting from the compression of hexagonal ice at 77 K can be converted to low density amorphous ice (LDA) by releasing the pressure at ≈ 115 K [12, 13, 14]. HDA and LDA can be inter-converted via an apparent first-order transition by applying or releasing pressure [11, 15]. Molecular dynamics simulations, based on different model potentials [16], have been able to reproduce the qualitative features of the crystalline ice-HDA, HDA-LDA, and LDA-HDA transitions [7, 9], even if the compression rates in simulations are several orders of magnitude larger than in experiments.

To study the LDA-HDA transition and the relation between glassy and liquid water we use tools that have been recently developed to study out-of-equilibrium liquids [17] in the potential energy landscape (PEL) framework [18, 19, 20]. In the PEL approach, the $6N$ -dimensional configurational space — defined by the $3N$ center of mass coordinates and by the $3N$ Euler angles, where N is the number of molecules — is partitioned into a set of basins, each of them associated with a different local minimum of the potential energy landscape. The set of points belonging to the same basin are those which, under a steepest descent minimization procedure, end up in the same local minimum. The local minima in the PEL are called inherent structures (IS). Each IS configuration is char-

acterized by its potential energy (e_{IS}), its pressure (P_{IS}) and by the $6N$ local curvatures of the PEL, which can be estimated in the harmonic approximation by diagonalizing the Hessian matrix [21]. Basins with different depths have different curvatures [22, 23, 24, 25]. One possible measure of the average basin curvature — the one used in the present work — is offered by the “shape function”

$$\mathcal{S}_{IS} \equiv \frac{1}{N} \sum_{i=1}^{6N-3} \ln \left(\frac{\hbar\omega_i}{A_0} \right), \quad (1)$$

where ω_i is the frequency of vibrational mode i [21], \hbar is the Planck constant, and $A_0 = 1$ kJ/mol. This choice is motivated by the fact that \mathcal{S}_{IS} enters into the evaluation of the basin free energy in the harmonic approximation [26].

Recent work has provided a detailed statistical description of the number, depth and shape of the basins, for models of both simple liquids [24, 26, 27] and molecular liquids [25, 28]. It has been shown that, on cooling, the liquid samples regions of the PEL characterized by lower and lower e_{IS} values [20] and that both P_{IS} and \mathcal{S}_{IS} are correlated with e_{IS} [29]. Numerical studies of the PEL sampled by the equilibrium liquid permit precise calculations of both $\mathcal{S}_{IS}(e_{IS}, \rho)$ and $P_{IS}(e_{IS}, \rho)$, providing a detailed description of the region of the PEL sampled under equilibrium conditions [23, 30, 31].

In this Letter we aim at comparing the properties of the PEL sampled during the LDA-HDA transition with the properties of the PEL explored by the equilibrium liquid. If the regions of PEL explored by the glass during the transition are identical [32] to the regions explored by the equilibrium liquid, we are entitled to connect the glass-glass transformation (GGT) to a transition taking place in the liquid state, supporting the hypothesis that the LDA-HDA transformation is an out-of-equilibrium manifestation of a liquid-liquid first order transition. We discover that during the transformation the system explores regions of the landscape which are

never explored in equilibrium, supporting the possibility that the LDA-HDA transformation and the liquid-liquid first order transition might be independent phenomena. In this respect, the LDA-HDA transformation observed in numerical simulations [7, 8, 9] should not be taken as proof of the existence of a liquid-liquid transition.

We perform molecular dynamics (MD) simulations of 216 molecules interacting via the simple point charge extended (SPC/E) model of water [33]. This model has been studied extensively; the ρ and T dependence of structural and dynamic properties in equilibrium have been calculated. We use a simulation time step of 1fs and long range forces are handled using the reaction field method. We identify the IS by minimizing the potential energy using a conjugate gradient minimization algorithm and calculate e_{IS} , S_{IS} , and P_{IS} in the resulting local minimum configuration. During the MD simulation, starting equilibrium configurations at $\rho = 0.9 \text{ g/cm}^3$ are either (a) decompressed to 0.8 g/cm^3 or (b) compressed to 1.4 g/cm^3 and then decompressed to 0.8 g/cm^3 . We simulate at both $T = 0 \text{ K}$ and $T = 77 \text{ K}$.

At 77 K we perform MD simulations using two different compression/decompression rates ($d\rho/dt = 5 \times 10^{-4} \text{ g/cm}^3/\text{ps}$ and $5 \times 10^{-5} \text{ g/cm}^3/\text{ps}$) and average over 16 different realizations. In the calculation at $T = 0 \text{ K}$, each step consists of a density change of either $\Delta\rho = 5 \times 10^{-4} \text{ g/cm}^3$ or $\Delta\rho = 5 \times 10^{-5} \text{ g/cm}^3$, followed by an energy minimization. At each step the system is compressed by $\Delta\rho$ and the center of mass of each molecule is isotropically scaled. Initial configurations are extracted from a pre-existing ensemble of IS generated by quenching equilibrium liquid configurations at $\rho = 0.90 \text{ g/cm}^3$ and $T = 220 \text{ K}$. At this state point, SPC/E describes the LDA structure accurately. Any low-temperature equilibrium configuration with density close to the LDA density could be used as a starting configuration.

Figure 1 shows the behavior of P_{IS} and e_{IS} for the compression and decompression of a single $T = 0 \text{ K}$ configuration. Following each density change, the system is displaced from the local minimum in the PEL and a steepest descent minimization is performed to bring the system to the new location of the minimum. e_{IS} and P_{IS} are continuously modified under the density changes, and the initial parts of the curves in Figs. 1a and 1b show such continuous modification. Above $\rho \approx 1.05 \text{ g/cm}^3$, this continuous, smooth process is interrupted by sudden changes in both P_{IS} and e_{IS} , clearly visible in Fig. 1. Figure 1c shows the squared distance between two IS differing by 10^{-2} g/cm^3 , $|\Delta R|^2 \equiv \frac{1}{N} \sum_{i=1}^N dr_i^2$, where dr_i is the displacement of the center of mass of the i -th molecule. We see that $|\Delta R|^2$ changes significantly when discontinuous jumps in P_{IS} and e_{IS} occur. Thus, as in silica [34, 35], these changes are due to a mechanical instability associated with the vanishing of the lowest frequency mode, which forces the system to abandon the previous unstable configuration in favor of a new basin.

Figure 2 shows P_{IS} , e_{IS} , and S_{IS} for both $T = 0 \text{ K}$ and $T = 77 \text{ K}$, averaged over 16 different realizations

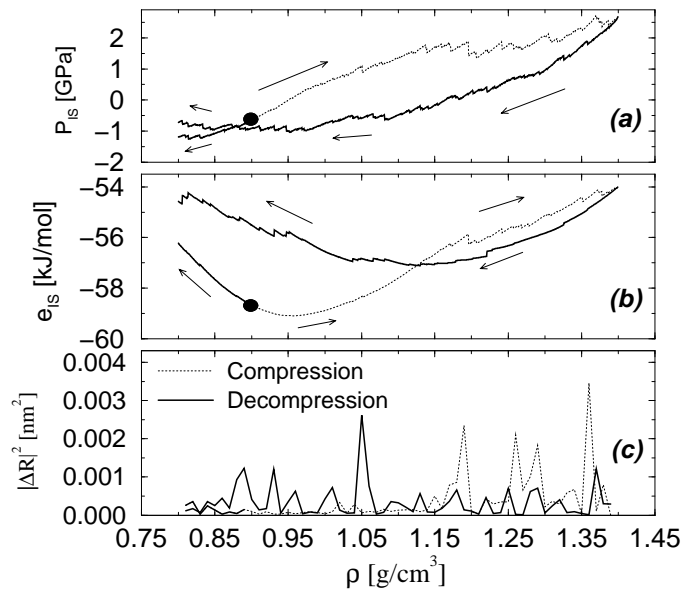


FIG. 1: (a) P_{IS} and (b) e_{IS} for $T = 0 \text{ K}$ as functions of ρ , where a starting glass configuration (black dot) is decompressed to $\rho = 0.8$, and also compressed to $\rho = 1.4 \text{ g/cm}^3$ and then decompressed to $\rho = 0.8 \text{ g/cm}^3$. The density in each step of the compression/decompression cycle is changed by $\Delta\rho = 5 \times 10^{-5} \text{ g/cm}^3$. (c) Squared distance between a sequence of IS configurations differing by 10^{-2} g/cm^3 along the compression/decompression path. Note the correlation between the large molecular rearrangements in part (c) and the corresponding discontinuities in P_{IS} and e_{IS} in part (a) and (b), such as one finds at $\rho = 1.20 \text{ g/cm}^3$.

as functions of ρ during compression and decompression at two different rates. The P_{IS} curve shows the typical behavior found for the pressure P observed in previous studies of compression and decompression of tetrahedral glasses [1, 7, 8, 14]. We find a strong hysteresis, an observation which has been interpreted as evidence in favor of a first order transition between two distinct structures, LDA and HDA [1, 7, 8].

On compressing, a significant flattening of P_{IS} is observed when the density becomes larger than $\approx 1.1 \text{ g/cm}^3$ at $T = 0 \text{ K}$ and larger than $\approx 1.0 \text{ g/cm}^3$ at $T = 77 \text{ K}$. At the beginning of the compression, the compression rate does not appear to play a significant role, but when the system is forced to change basins (due to thermal effects or mechanical instabilities) the compression rate becomes quite relevant. For the smaller compression rate, P_{IS} and e_{IS} are slightly smaller.

We next compare our results for $T = 0 \text{ K}$ and $T = 77 \text{ K}$. Transitions at $T = 0 \text{ K}$ are driven by the vanishing of the lowest normal mode frequencies resulting in the compression-induced disappearance of the explored basin. From the top panel of Fig. 2 we see that even though both systems start from the same configuration (and hence same IS) at $\rho = 0.9 \text{ g/cm}^3$, the additional thermal energy of the 77 K system enables the escape from the starting basin to occur at a smaller density.

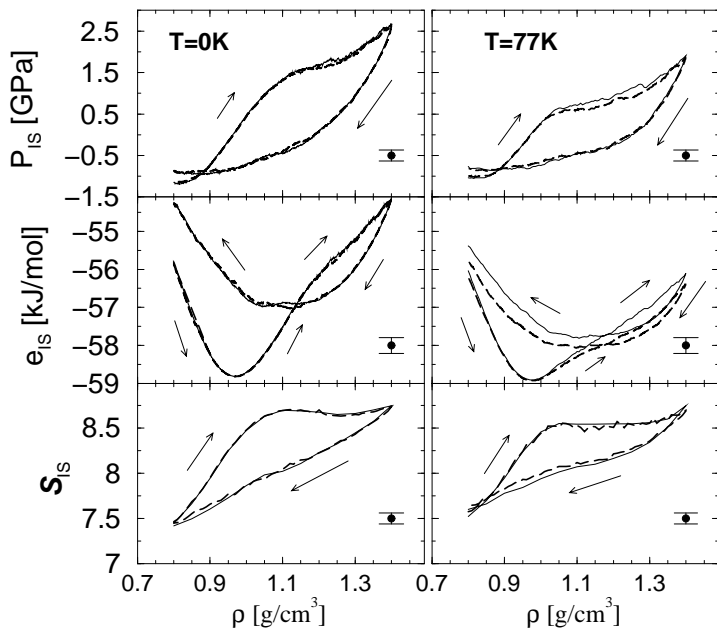


FIG. 2: P_{IS} , e_{IS} , and S_{IS} , averaged over 16 different realizations, as functions of ρ during the compression and decompression at $T = 0$ K (left panels) and $T = 77$ K (right panels) for the fast (solid line) and slow (dashed line) compression rates. Error bars are shown on the left lower corner.

This results in a more effective relaxation process and, correspondingly, in a flattening of P_{IS} at a smaller density value (compared to the $T = 0$ K case) and in smaller P_{IS} and e_{IS} values. The shape of the basin is also significantly modified by the compression/decompression cycle. We also find that the basin shape S_{IS} increases on compression and decreases on decompression, coherent with the frequency shifts of the translational peaks of the density of states (i.e. in the probability distribution for ω_i). In the region where P_{IS} flattens, neither S_{IS} nor the density of states changes significantly.

After a complete compression/decompression cycle, the system does not return to the same configuration. Indeed, Fig. 2 shows that while P_{IS} has the same value on compression and decompression at $\rho \approx 0.89$ g/cm³, the values for e_{IS} and S_{IS} differ—i.e., at $\rho \approx 0.89$ g/cm³, T and P are identical, but quite significant differences are detected at a microscopic level. This finding supports the interesting possibility that more than one significantly different configuration corresponds to LDA.

We next compare PEL properties sampled in equilibrium at different T and ρ with PEL properties sampled by the glass during the compression/decompression path with the slow compression rate. Figure 3 contrasts P_{IS} and S_{IS} in an equilibrium liquid (solid symbols) [30] and during the compression/decompression runs (open symbols) at $T = 77$ K. Surprisingly, we find that even a slight density change (from $\rho = 0.9$ to 1.0 g/cm³) allows the system to begin exploring regions of configuration space not explored under equilibrium conditions at the corre-

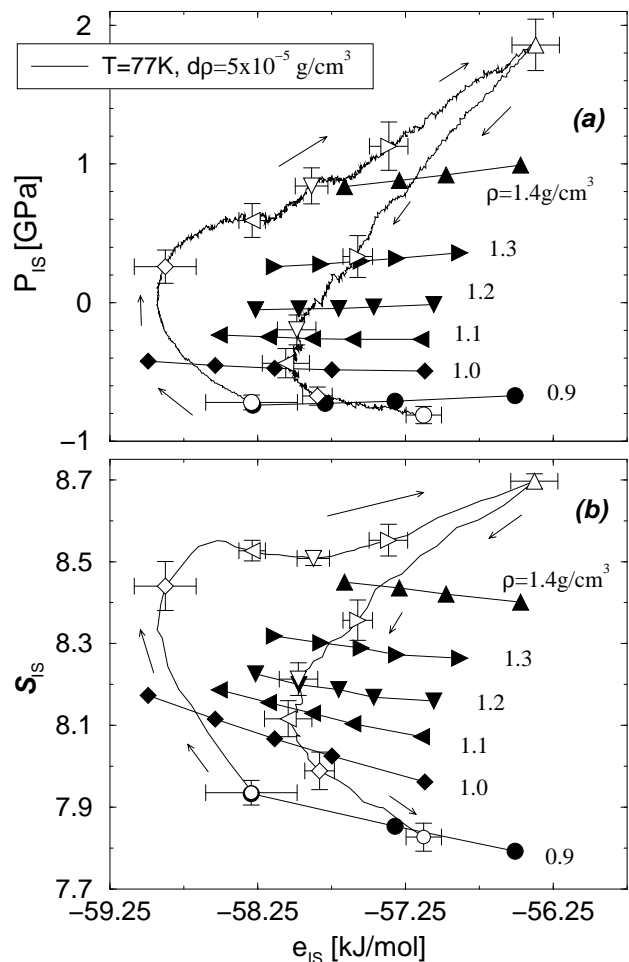


FIG. 3: (a) P_{IS} and (b) S_{IS} as functions of e_{IS} at different densities for the equilibrium liquid (filled symbols) and for the compression/decompression of glass (thin line) at both temperatures studied. Open symbols indicate the density during the compression/decompression. The relative location of the open symbol with respect to the location of the same filled symbol is a measure of the difference between the landscape properties in equilibrium and in the glass. The significant difference in the location confirms that the compressed/decompressed glass explores PEL regions not explored under equilibrium conditions at the same density. Densities are 0.9(\circ), 1.0(\diamond), 1.1(\triangleleft), 1.2(∇), 1.3(\triangleright), and 1.4(\triangle) g/cm³. The error bars for these densities are indicated in the figures. Data for equilibrium liquid are averaged over 2000 realizations and error bars are smaller than the corresponding symbol size.

sponding density. For a given ρ , P_{IS} and S_{IS} are larger in the compressed glass than observed under equilibrium liquid conditions. We find that the $T = 0$ K results show even larger differences.

For small density changes ($\rho \lesssim 1.1$ g/cm³ at $T = 0$ K, or for $\rho \lesssim 1.0$ g/cm³ at $T = 77$ K) the system is still confined in the (deformed) starting basin. In this density range (i.e., before any basin change) compression rate effects do not play any role. Figure 3 shows that even be-

fore basin change effects become relevant, the system is already in a compressed state which hardly remembers an equilibrium liquid configuration. The values of P_{IS} and \mathcal{S}_{IS} at $\rho = 1.0 \text{ g/cm}^3$ are comparable to the equilibrium liquid values corresponding to a much higher density of 1.3 g/cm^3 . Hence we conclude that the flattening of the P_{IS} curve of Fig. 2—associated with the LDA-HDA transition—takes place in a region of the PEL that is never explored under equilibrium conditions.

Our results support the view that the compression/decompression of glassy water takes place along a PEL path rarely explored by the equilibrium liquid. Such information — which could not have been extracted from standard analysis (such as standard thermodynamic or structural quantities) — is made possible by the extreme sensitivity of the landscape properties. We have shown that the IS visited by the liquid (on the time scale probed in computer simulations) are different than those sampled by the glass. This observation has profound consequences for the possibility of developing a thermodynamic approach to the LDA-HDA transformation. Indeed, only when the glass state can be associated with a frozen liquid (i.e. when the equilibrium relations $\mathcal{S}_{\text{IS}}(e_{\text{IS}}, \rho)$ and $P_{\text{IS}}(e_{\text{IS}}, \rho)$ are satisfied) it becomes possible to provide a thermodynamic description of the glass and formally connect the mechanical instability of the LDA-HDA transformation to a mechanical instability in

the liquid state[17, 26]. If the liquid and the glass had shared the same portion of the PEL, then the mechanical instability observed during the transformation would have constituted genuine evidence of a liquid-liquid transition. The observation that the LDA-HDA transformation is unrelated to properties of the equilibrium liquid [36] does not allow us to relate the observed numerical GGT to a liquid-liquid transition. Due to the extremely different time scales probed in experiments and in simulations, our numerical results do not exclude neither the existence of a liquid-liquid transition nor the possibility that the LDA-HDA transition observed experimentally is related to a liquid-liquid transition. Our results show that the PEL properties at the beginning and the end of the compression/decompression cycle are different, suggesting that several distinct configurations can be associated with LDA.

Acknowledgments

We thank NSF Chemistry Program, MIUR Cofin 2002 and Firb and INFN Pra GenFdt for support and SHARCNET and BU Computation Center for a generous allocation of CPU time. FS thanks UWO for its hospitality.

-
- [1] O. Mishima, *J. Chem. Phys.* **100**, 5910 (1993).
 [2] O. Mishima and H. E. Stanley, *Nature* **392**, 164 (1998).
 [3] T. Loerting *et al.*, *Phys. Chem. Chem. Phys.* **3**, 5355 (2001).
 [4] C. A. Tulk *et al.*, *Science* **297**, 1320 (2002).
 [5] T. Loerting *et al.*, *J. Chem. Phys.* **116**, 3171 (2002).
 [6] J. L. Finney *et al.*, *Phys. Rev. Lett.* **89**, 205503 (2002).
 [7] J. S. Tse and M. L. Klein, *Phys. Rev. Lett.* **58**, 1672 (1987).
 [8] P. H. Poole *et al.*, *Nature* **360**, 324 (1992).
 [9] P. H. Poole *et al.*, *Phys. Rev. E* **48**, 4605 (1993).
 [10] J. S. Tse *et al.*, *Nature* **400**, 647 (1999).
 [11] O. Mishima *et al.*, *Nature* **314**, 76 (1985).
 [12] O. Mishima *et al.*, *Nature* **310**, 393 (1984).
 [13] Y. P. Handa, *et al.*, *J. Chem. Phys.* **84**, 2766 (1986).
 [14] M. A. Floriano *et al.*, *J. Chem. Phys.* **91**, 7187 (1989).
 [15] O. Mishima *et al.*, *Science* **254**, 406 (1991).
 [16] Previous simulations on the LDA-HDA transformation were done using the TIP4P[7] and ST2[9] models.
 [17] S. Mossa *et al.*, *Eur. Phys. J. B* **30**, 351 (2002).
 [18] M. Goldstein, *J. Chem. Phys.* **51**, 3728 (1969).
 [19] F. H. Stillinger and T. A. Weber, *Phys. Rev. A* **28**, 2408 (1983); C. A. Angell, *Science* **267**, 1924 (1995).
 [20] S. Sastry *et al.*, *Nature* **393**, 554 (1998).
 [21] To obtain ω_i , we first calculate the $6N \times 6N$ matrix of the second derivatives of the potential energy with respect to the $6N$ coordinates of the molecules, evaluated at the IS configuration. Then we diagonalize the matrix. The i -th eigenvalue is ω_i^2 . Physically it indicates the local curvature of the PEL at the IS along the direction of the i -th eigenvector of the matrix. The probability distribution for ω_i defines the vibrational density of states.
 [22] W. Kob *et al.*, *Eur. Phys. Lett.* **49**, 590 (2000).
 [23] F.W. Starr *et al.*, *Phys. Rev. Lett.* **63**, 041201 (2001).
 [24] S. Sastry, *Nature* **409**, 164 (2001).
 [25] S. Mossa *et al.*, *Phys. Rev. E* **65**, 041205 (2002).
 [26] F. Sciortino and P. Tartaglia, *Phys. Rev. Lett.* **86**, 107 (2001); F. Sciortino *et al.*, *ibid.* **83**, 3214 (1999).
 [27] I. Saika-Voivod *et al.*, *Nature* **412**, 514 (2001).
 [28] F. W. Starr *et al.*, *Phys. Rev. E* **63**, 041201 (2001).
 [29] E. La Nave *et al.*, *Phys. Rev. Lett.* **88**, 225701 (2002).
 [30] E. La Nave *et al.*, preprint. The relations $\mathcal{S}_{\text{IS}}(e_{\text{IS}}, \rho)$ and $P_{\text{IS}}(e_{\text{IS}}, \rho)$ from equilibrium systems are estimated along an isochore as follows. First, we generate set of 2000 independent equilibrium configuration, with standard MD, at several different T . All configurations are then minimized to generate the associated IS. For each T , the average values of P_{IS} , \mathcal{S}_{IS} and e_{IS} are then calculated, averaging over the generated inherent structures set.
 [31] P.G. Debenedetti *et al.*, *J. Phys. Chem. B* **103**, 7390 (1999).
 [32] The word *identical* means that e_{IS} , \mathcal{S}_{IS} , and P_{IS} along the GGT satisfy the equilibrium functional forms $\mathcal{S}_{\text{IS}}(e_{\text{IS}}, \rho)$ and $P_{\text{IS}}(e_{\text{IS}}, \rho)$.
 [33] H. J. Berendsen *et al.*, *J. Phys. Chem.* **91**, 6269 (1987).
 [34] D. L. Malandro and D. J. Lacks, *J. Chem. Phys.* **107**, 5804 (1997); D. J. Lacks, *Phys. Rev. Lett.* **80**, 5385 (1998);
 [35] D. J. Lacks, *Phys. Rev. Lett.* **84**, 4629 (2000).
 [36] E. A. Jagla, *Phys. Rev. Lett.* **86**, 3206 (2001).